Chinese Chemical Letters 34 (2023) 108317

Contents lists available at ScienceDirect

Chinese Chemical Letters

journal homepage: www.elsevier.com/locate/cclet

Ru/Pt@BSA nanoparticles for efficient photo-catalytic oxidation of NAD(P)H and targeted cancer treatment under hypoxic conditions

Xuwen Da, Xiulian Liu, Chao Li, Yatong Peng, Yao Jian, Wanpeng Zhou, Yunli Xu, Yao Wu, Xuesong Wang*, Qianxiong Zhou*

Key Laboratory of Photochemical Conversion and Optoelectronic Materials, Technical Institute of Physics and Chemistry, Chinese Academy of Sciences, Beijing 100190, China

ARTICLE INFO

Article history:
Received 29 December 2022
Revised 1 March 2023
Accepted 7 March 2023
Available online 12 March 2023

Keywords:
Hypoxic
Cancer treatment
Photo-catalytic oxidation NAD(P)H
Cyclic utilization of oxygen
Pt nanoparticle

ABSTRACT

Photo-catalytic oxidation of intracellular nicotinamide adenine dinucleotide (2′-phosphate) (NAD(P)H) has attracted much attention for cancer therapy. However, the general oxygen-dependent mechanism heavily depresses the efficacy in hypoxic tumors. To solve this problem, herein platinum nanoparticles (Pt NPs) with catalase-like (CAT-like) and catalytic H_2 evolution activities were introduced as a powerful assistant to enhance the photo-catalytic NAD(P)H oxidation of Ru1 ($[Ru(phen)_2(PIP\text{-}OCH_3)]^{2+}$, phen = 1,10-phenanthroline, PIP-OCH_3 = 2-(4–methoxy phenyl)-1*H*-imidazo[4,5-*f*][1,10]phenanthroline) under hypoxic and even oxygen-free conditions. Firstly, Pt NPs can transform the original and *in situ* formed H_2O_2 once again into O_2 by the CAT-like activity, thus relieving tumor hypoxia and realizing cyclic utilization (at least in part) of the precious oxygen in hypoxia. Secondly, Pt NPs can also be served as H_2 evolution catalysts while using Ru1 as the photosensitizer and NAD(P)H as the electron and proton donor. In this process, NAD(P)H is oxidized without the participation of oxygen, which can provide an effective way even under oxygen-free conditions. *Via* co-encapsulation of Ru1 and Pt NPs in bovine serum albumin (BSA) with tumor targeting ability, the resultant Ru/Pt@BSA could photo-catalyze intracellular NAD(P)H oxidation under hypoxic conditions (3% O_2), and exhibited an efficient and selective anticancer activity both *in vitro* and *in vivo*. Our results may provide new sights for efficient and targeted cancer treatment under hypoxic conditions.

Cancer has become a major threat to human health and survival [1–3]. Surgery, chemotherapy and radiotherapy are the most widely used cancer treatments in clinic [4–6]. However, the severe side effects and unsatisfactory prognosis are still commonplace things [7–9]. Thus, it is urgent to develop new cancer treatment tactics with high efficiency and selectivity [10]. Phototherapy which can control the drug activity in a spatiotemporal manner has attracted much attention in the past decades [11–15]. Recently, photo-catalytic oxidation of intracellular reduced nicotinamide adenine dinucleotide (2′-phosphate) (NAD(P)H) [16], as a novel type of photo-catalytic anticancer mechanism of action, was proposed. NAD(P)H plays vital roles in intracellular energy production, biomolecules (lipid, nucleus acid, cholesterol, *etc.*) synthesis, maintenance of redox homeostasis and so on [17,18]. Therefore, photo-catalytic depletion of intracellular NAD(P)H can lead to cancer cell death. Some metal (Ir(III) [19–21], Ru(II) [22–25]) and metal-free compounds [26–28], which are able to efficiently photo-oxidize NAD(P)H have shown good anticancer activity both *in vitro* and *in vivo*.

Generally, photo-catalytic oxidation of NAD(P)H is an oxygen-dependent process as demonstrated in Scheme S1A (Supporting information) [25], taking a Ru(II) photosensitizer as an example. NAD(P)H is photo-catalytically oxidized into $NAD(P)^+$, and H_2O_2 is generated when O_2 acts as the electron and proton acceptor. However, considering that many tumors are in a hypoxic microenvironment [29–32], the efficacy of the above-mentioned process and consequent therapeutic outcomes may be heavily depressed. Hence to realize effective NAD(P)H photo-oxidation under hypoxic conditions is quite important to strengthen the power of this anticancer mechanism of action. Many efforts have been made to relieve tumor hypoxia, including developing type-I photosensitizers [33,34], introducing oxygen carriers [35] and so on [36]. Sadler [16], Peng and coauthors [27] have reported that NADH can be photo-catalytically oxidized using hemoprotein Cyt *c* (Fe^{3+}) as

* Corresponding authors.
E-mail addresses: xswang@mail.ipc.ac.cn (X. Wang), zhouqianxiong@mail.ipc.ac.cn (Q. Zhou).

https://doi.org/10.1016/j.cclet.2023.108317
1001-8417/

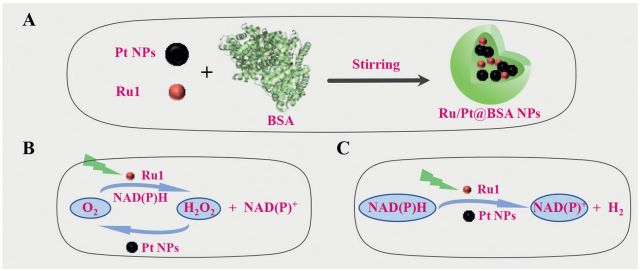

Scheme 1. Schematic illustration of fabrication of Ru/Pt@BSA (A), and the postulated mechanism of photo-catalytic oxidation of NAD(P)H under hypoxic and oxygen-free conditions (B and C).

the electron acceptor in degassed solutions, which may provide a possible O_2-independent pathway in cells. Good subcellular co-localization of the photo-catalysts and hemoprotein Cyt *c* (generally in mitochondria for living cells) is necessary to realize such an efficient electron transfer. However, this may not be the case for many photo-catalysts as they may not accumulate in mitochondria.

In our previous work, we have reported a series of Ru(II)-based photosensitizers, among which Ru1 ($[Ru(phen)_2(PIP\text{-}OCH_3)]^{2+}$, phen = 1,10-phenanthroline, PIP-OCH_3 = 2-(4–methoxy phenyl)-1*H*-imidazo[4,5-*f*][1,10]phenanthroline) (Scheme S2 in Supporting information) displayed the most efficient photo-catalytic NAD(P)H oxidation activity under aerobic conditions, accompanied by the production of H_2O_2 with a high yield of 73.2% [25]. To regain the glory under hypoxic or even oxygen-free conditions, herein ultrasmall platinum nanoparticles (Pt NPs) were introduced as a powerful assistant to realize such a goal. Our idea is mainly based on the following considerations: (1) the catalase (CAT)-like activity of Pt NPs is well known [37–39], and can be utilized to re-transform the *in situ* generated H_2O_2 into oxygen during the photo-catalytic process, thereby achieving cyclic utilization (at least in part) of the precious oxygen in hypoxia (Scheme 1B and Scheme S1B in Supporting information). Moreover, H_2O_2 is usually over-expressed in tumor cells [30,40], which is very helpful to alleviate hypoxia by the aid of CAT-like activity of Pt NPs *in vitro* and *in vivo*. (2) Pt NPs can also be served as H_2 evolution catalysts (HEC) while using Ru1 as the photosensitizer and NAD(P)H as the electron and proton donor (Scheme 1C and Scheme S1B) [41,42]. In this process, NAD(P)H is oxidized without the participation of oxygen, which may provide an effective way even under oxygen-free conditions. *Via* further co-encapsulation of Ru1 and Pt NPs in bovine serum albumin (BSA) (Scheme 1A), the resultant Ru/Pt@BSA nanoparticles can photo-catalyze NAD(P)H oxidation in hypoxic and Ar-saturated solutions. Thanks to the tumor targeting ability of BSA which shows high binding affinity towards glycoprotein 60 (gp60) overexpressed on the membranes of many cancer cells [18,43,44], Ru/Pt@BSA exhibits targeted and efficient anticancer activity both *in vitro* and *in vivo* upon visible light irradiation. For comparison, Ru@BSA and Pt@BSA were also constructed and studied in detail.

Pt NPs were prepared based on the reported method [45–47]. The obtained Pt NPs are ultrasmall with a diameter of about 3–5 nm, and the 0.2 nm lattice spacing is visible under transmission electron microcopy (TEM) (Figs. 1A and B). The energy-dispersive X-ray spectroscopy (EDS) elemental analysis clearly shows Pt-based signals (Fig. S1 in Supporting information). Moreover, the zeta potential of Pt NPs was −34.0 mV (Fig. S2 in Supporting information). The above results are consistent with the reported data and indicate the successful synthesis of Pt NPs [45].

The CAT-like activity of Pt NPs was investigated by the ability to convert hydrogen peroxide into oxygen. As shown in Fig. S3 (Supporting information), a lot of oxygen bubbles could be observed for the mixture containing both Pt NPs and H_2O_2, while none appeared for the solutions of either Pt NPs or H_2O_2 under the same conditions. The resulted oxygen was further quantified by Clark oxygen electrode. As shown in Fig. 1C, the concentration of oxygen increased sharply as soon as H_2O_2 was added into the Pt solution. About 700 nmol O_2 was generated after adding 1.5 μmol H_2O_2, corresponding to a yield of about 93.3% (two H_2O_2 can theoretically generate one O_2). These results indicate that Pt NPs possess good CAT-like activity.

Our previous study has shown that Ru1 can efficiently photocatalyze NAD(P)H oxidation and produce H_2O_2 *in situ* with a high yield of 73.2% under aerobic conditions [26]. To combine Ru1 with Pt NPs may be a good choice to convert the *in situ* generated H_2O_2 once again into O_2, thus realizing partial cyclic utilization of limited oxygen in hypoxia. Thus, Pt NPs and Ru1 were further co-loaded in BSA to take full advantage of its cancer targeting ability. The obtained Ru/Pt@BSA NPs were characterized by TEM, dynamic light scattering (DLS), absorption and emission spectra. As shown in Fig. 1D, Ru/Pt@BSA has a uniform size with an average diameter of about 41 nm. The scanning transmission electron microscopy (STEM) and the EDS elemental mapping images clearly showed the presence of Ru- and Pt-based signals along with that based on S and P elements (Figs. S4 and S5 in Supporting information). The DLS result exhibits a mean hydrodynamic diameter of about 79.2 ± 1.2 nm (Fig. S6A in Supporting information), which is larger than the TEM result probably due to the water layer outside the particles. Ru/Pt@BSA displays the combined absorption of Ru1 and Pt NPs, and Ru1 based emission peak at 605 nm (Figs. 1E and F), confirming the successful co-loading of Ru1 and Pt NPs. For comparison, BSA nanoparticles loaded with only Ru1 (Ru@BSA) or Pt NPs (Pt@BSA) were also prepared and characterized by absorption spectra (Fig. S7 in Supporting information). The DLS results showed that the diameters of Ru@BSA and Fe@BSA were about 70.3 ± 0.7 nm and 66.8 ± 1.0 nm, respectively (Figs. S6B and C in Supporting information). Using inductive coupled plasma atomic emission spectrometry (ICP-AES) to measure the Ru and Pt contents, the loading rate of Ru1 in Ru/Pt@BSA and Ru@BSA is quantified to be about 3.9 wt%, and that of Pt in Ru/Pt@BSA and Pt@BSA is about 8.5 wt%.

The CAT-like activity of Pt NPs maintaines very well after encapsulation in BSA. As shown in Fig. S8 (Supporting information), oxygen bubbles are visible to the naked eyes for Pt@BSA and Ru/Pt@BSA solutions after adding H_2O_2. Control experiments indicate Pt NPs are necessary to decompose H_2O_2.

The photo-catalytic NADH oxidation activities of Ru@BSA and Ru/Pt@BSA were compared under different conditions. The typical absorption peak at about 336 nm of NADH disappears after oxidation into NAD^+, which can be readily utilized to monitor the oxidation process. As shown in Fig. S9 (Supporting information), both Ru/Pt@BSA and Ru@BSA could photo-catalyze NADH oxidation efficiently under aerobic conditions. Ru@BSA and Ru/Pt@BSA (5 μmol/L based on Ru1) could lead to almost full oxidation of NADH (200 μmol/L) after 3 min of irradiation (470 nm, 22.5 mW/cm^2). After that, hydrogen peroxide was detected for Ru@BSA by test paper (inset of Fig. S9A), but almost none was observed for Ru/Pt@BSA (inset of Fig. S9B) due to the presence of Pt NPs with CAT-like activity. Under hypoxic conditions (3% O_2), the photo-catalytic NADH oxidation induced by Ru/Pt@BSA was much faster than that by Ru@BSA (Figs. 2A and B, 5 μmol/L based on Ru1 for both). Efficient conversion of the *in situ* generated H_2O_2 once again into O_2 should play an important role for the enhanced activity of Ru/Pt@BSA under hypoxic conditions. Moreover, considering that H_2O_2 is usually over-expressed in many cancer cells, we further examined the photo-catalytic performances in Ar-saturated solutions by adding different concentrations of H_2O_2. As shown in Fig. 2C and Fig. S10 (Supporting information), Ru/Pt@BSA can photo-catalyze NADH oxidation in a H_2O_2 concentration-dependent manner, which is

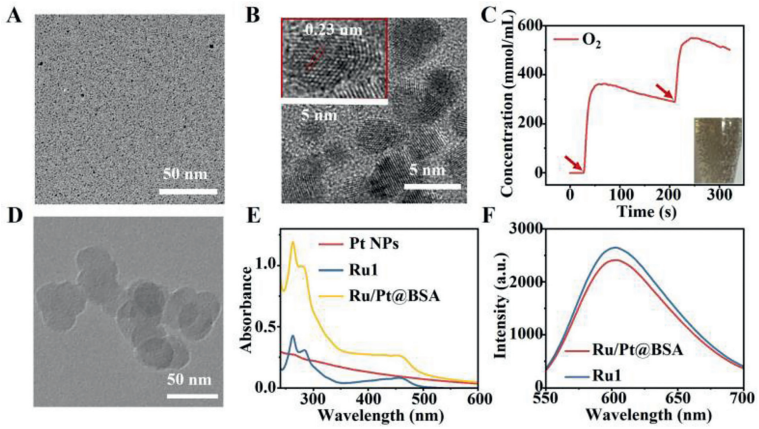

Fig. 1. (A, B) TEM images of Pt NPs, (C) O_2 evolution detected by Clark electrode after adding H_2O_2 into a Pt NPs solution (30 μg/mL). The arrow indicates H_2O_2 was added. Inset shows formation of oxygen bubbles. (D) TEM image of Ru/Pt@BSA. (E) Absorption spectra of Pt NPs, Ru1 and Ru/Pt@BSA. (F) Emission spectra of Ru1 and Ru/Pt@BSA upon 470 nm excitation.

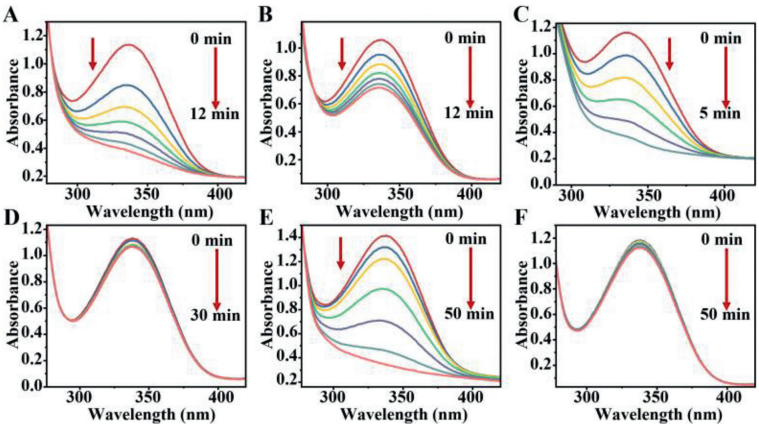

Fig. 2. Photo-induced (470 nm, 22.5 mW/cm^2) absorption spectral changes of NADH (200 μmol/L in H_2O) in the presence of Ru/Pt@BSA (Ru1: 5 μmol/L, Pt: 10 μg/mL) or Ru@BSA (Ru1: 5 μmol/L) under different conditions. (A) In the presence of Ru/Pt@BSA and (B) Ru@BSA under hypoxic conditions (3% O_2); (C) In the presence of Ru/Pt@BSA and (D) Ru@BSA in Ar-saturated solutions with addition of 1 mmol/L H_2O_2; (E) In the presence of Ru/Pt@BSA and (F) Ru@BSA in Ar-saturated solutions.

consistent with the efficient CAT-like activity of Pt NPs. Interestingly, in the absence of H_2O_2, Ru/Pt@BSA can still photo-catalyze NADH oxidation in an Ar-saturated solution (Fig. 2E). Ru/Pt@BSA (5 μmol/L based on Ru1) can lead to a full oxidation of NADH (200 μmol/L) after 50 min of irradiation (470 nm, 22.5 mW/cm^2). As expected, Ru@BSA almost lost the ability under the same conditions (Figs. 2D and F, Fig. S11 in Supporting information). In this case, we deduce the Pt NPs act as H_2 evolution catalysts, while Ru1 is the photosensitizer and NADH is the electron and proton donor. After full reaction, H_2 appeared at the top of a sealed cuvette and could be detected by gas chromatography (Fig. S12 in Supporting information). Such a process is totally oxygen-independent, which may provide another possibility to enhance the photo-catalytic NADH oxidation by Ru1 under hypoxic conditions.

In addition, Ru1 is also a good singlet oxygen generator with a quantum yield of about 0.94 in air-saturated solutions [22]. In Ar-saturated solutions, singlet oxygen production of Ru@BSA is significantly inhibited using ABDA as the singlet oxygen trap (Fig. S13B in Supporting information). By adding H_2O_2 (0.5 mmol/L) into the Ar-saturated solutions, singlet oxygen production of only Ru/Pt@BSA recovered due to the supplement of O_2 by Pt NPs (Fig. S13A in Supporting information). Thus, in the hypoxic microenvironment of tumor tissues with overexpressed H_2O_2, Ru/Pt@BSA may kill cancer cells in multiple pathways as mentioned above.

The results in solutions encourage us to investigate their performance in cells. Firstly, O32 (hydrogen peroxide fluorescence probe) which can specifically react with H_2O_2 and emit green fluorescence was used to detect the intracellular H_2O_2 by confocal microscopy. Under normoxic conditions, strong green fluorescence was observed for the A549 (human lung cancer) cells treated by Ru@BSA upon 470 nm light irradiation (Fig. S14 in Supporting information), indicating the production of H_2O_2 *in situ* through the photo-catalytic oxidation of intracellular NAD(P)H. The control experiments display that Ru1 and light irradiation are necessary. However, only faint fluorescence appeared for the Ru/Pt@BSA and light treated cells, which can be ascribed to the co-loaded Pt NPs with efficient CAT-like activity. In addition, H_2O_2 is usually overexpressed in cancer cells as stated earlier, and can also be utilized to alleviate hypoxia. To confirm this, $[Ru(dpp)_3]Cl_2$ (dpp = 4,7-diphenyll-1,10-phenanthroline) was used as an oxygen probe to detect the intracellular O_2 levels by confocal microscopy under hypoxic conditions (3% O_2). High levels of oxygen can quench the red emission of $[Ru(dpp)_3]Cl_2$. As shown in Fig. S15 (Supporting information), obvious red luminescence was observed for the A549 cells treated by Ru@BSA, hinting at a low oxygen level. The red emission was largely quenched for the cells treated with Ru/Pt@BSA, which indicates an elevated O_2 level induced by co-loaded Pt NPs. These results confirm that Pt NPs can efficiently transform the original or *in situ* produced H_2O_2 into O_2 in cells, thus is helpful to alleviate tumor hypoxia.

Intracellular NAD(P)H levels of A549 cells upon different treatments under hypoxic conditions (3% O_2) were further investi-

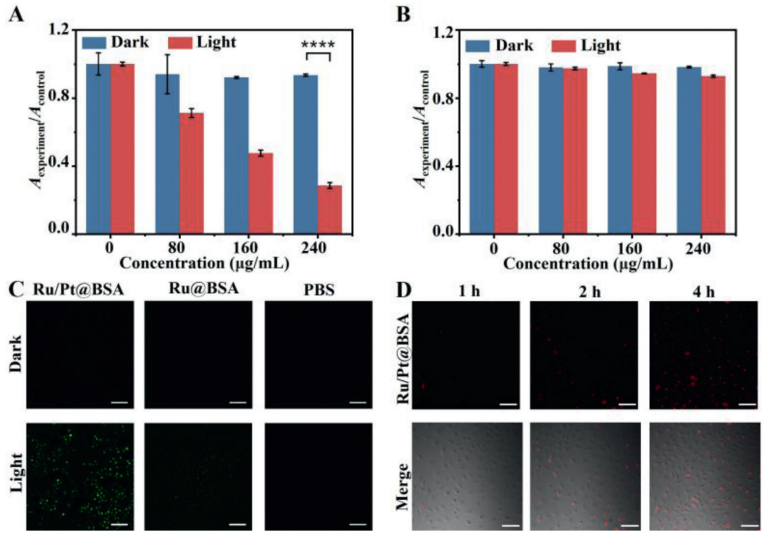

Fig. 3. NAD(P)H levels of A549 cells treated with varied concentrations of Ru/Pt@BSA (A) or Ru@BSA (B) with or without irradiation under hypoxic conditions. Each experiment was carried out in triplicate, and data are expressed as mean ± standard deviation (SD) ($n = 3$) ($^{****}P < 0.0001$, two-tailed Student's *t*-test). (C) Intracellular ROS levels of A549 cells treated with Ru/Pt@BSA, Ru@BSA or phosphate buffer saline (PBS) in the dark or upon light irradiation under hypoxic conditions. DCFH-DA was used as the fluorescent probes. Irradiation conditions: 470 nm, 22.5 mW/cm^2, 30 min. (D) Confocal luminescence images of A549 cells treated with Ru/Pt@BSA for different times. Scale bar: 100 μm.

gated using commercial NAD(P)H detection kits. As shown in Fig. 3A, Ru/Pt@BSA displayed negligible effects in the dark, but could decrease the intracellular NAD(P)H levels in a concentration-dependent manner upon 470 nm irradiation (22.5 mW/cm^2 for 30 min). Specifically, the NAD(P)H level reduced by 72% after treating with 240 μg/mL of Ru/Pt@BSA (about 10.5 μmol/L based on Ru1). On the contrary, almost no effects were observed for Ru@BSA under the same conditions (Fig. 3B). These results highlight the important role of Pt NPs in enhancing the photo-catalytic activity of Ru1 in hypoxia, *i.e.* the CAT-like activity can alleviate tumor hypoxia, and the HEC activity may endow Ru/Pt@BSA an oxygen-independent pathway to oxidize intracellular NAD(P)H.

The total intracellular reactive oxygen species (ROS) levels of A549 cells were examined using 2′,7′-dichlorodihydrofluorescein diacetate (DCFH-DA) as a probe. DCFH-DA is not emissive but can be oxidized into fluorescent 2′,7′-dichlorofluorescein (DCF) by intracellular ROS. Under normoxic conditions, quite weak green fluorescence appeared for the A549 cells treated by Ru@BSA (about 350 nmol/L based on Ru1) and 470 nm light irradiation (22.5 mW/cm^2 for 30 min), while much stronger fluorescence was observed for Ru/Pt@BSA under the same conditions (Fig. S16 in Supporting information). We deduce that the photo-catalytic process quickly consumes the intracellular O_2 to produce H_2O_2, while Ru/Pt@BSA can supplement O_2 in time to amplify the ROS levels. Under hypoxic conditions, similar trends were observed. A549 cells treated by Ru/Pt@BSA (about 3.5 μmol/L based on Ru1) upon irradiation displayed obvious green fluorescence, which was quite faint for Ru@BSA treated cells under the same conditions (Fig. 3C).

The results above prove that the presence of Pt NPs can significantly enhance the photo-catalytic oxidation of intracellular NAD(P)H and ROS production, which stimulates us to further investigate the anticancer activity *in vitro* and *in vivo*. A standard methyl thiazolyl tetrazolium (MTT) assay was employed to evaluate the cytotoxicity against cancer cells (including A549 and HeLa (human cervical cancer)) and IOSE80 normal cells (human normal ovarian epithelial). As shown in Fig. S17 (Supporting information), no obvious dark cytotoxicity was observed for Ru@BSA and Ru/Pt@BSA towards A549 and HeLa cells. Upon 470 nm irradiation (22.5 mW/cm^2 for 30 min) under normoxic conditions, Ru@BSA displayed good anticancer activity with half maximal inhibitory concentration (IC_{50}) values about 24 μg/mL (1.0 μmol/L in Ru1) and 19 μg/mL (0.8 μmol/L in Ru1) towards A549 and HeLa cells, respectively. Ru/Pt@BSA exhibited much enhanced photo-toxicity under the same conditions, yielding IC_{50} values about 8 μg/mL (about 350 nmol/L in Ru1) and 7 μg/mL (about 300 nmol/L in Ru1) towards A549 and HeLa cells, respectively. Under hypoxic conditions, the photo-toxicity of both Ru@BSA and Ru/Pt@BSA was depressed, while that of the latter was relatively less effected. The IC_{50} values of Ru@BSA towards A549 cells are about 376 μg/mL (16 μmol/L in Ru1). These data are about 20 times that under normoxic conditions. While for Ru/Pt@BSA, the IC_{50} values towards A549 in hypoxia upon irradiation are only about 10 times (about 82 μg/mL (3.5 μmol/L in Ru1) that in normoxia (Fig. S18 in Supporting information). The presence of Pt NPs can significantly enhance the photo-toxicity, which is consistent with the improved photo-catalytic oxidation of intracellular NAD(P)H and ROS generation.

It is worth noting that Ru/Pt@BSA had much lower photo-cytotoxicity towards normal IOSE80 cells with an IC_{50} value about 235 μg/mL (10 μmol/L in Ru1) under normoxic conditions (Fig. S19 in Supporting information), which can be ascribed to the cancer targeting ability of BSA by specific interaction with gp60 overexpressed on the membranes of tumor cells [15,36,37]. As shown in Fig. 3D, the intracellular red luminescence of Ru1 gradually increased with the extension of incubation time, which indicates Ru/Pt@BSA NPs was gradually internalized by A549 cells. However, under the same conditions, poor uptake was observed for the normal IOSE80 cells as little red luminescence appeared (Fig. S20 in Supporting information). The good cancer targeting ability of Ru/Pt@BSA can minimize the possible side effects further.

Moreover, calcein-AM (staining live cells with green fluorescence) and PI (staining dead cells with red fluorescence) were used to visualize the live and dead cells after different treatments under hypoxic conditions (3% O_2). As shown in Fig. S21 (Supporting information), almost all the A549 cells treated with Ru/Pt@BSA (240 μg/mL) and 470 nm light irradiation (22.5 mW/cm^2 for 30 min) were stained by PI with red fluorescence, *i.e.* dead. Only faint red fluorescence was observed for Ru@BSA under the same conditions, indicating much lower photo-cytotoxicity of Ru@BSA. No obvious red fluorescence was detected for the cells treated with Pt@BSA in the dark or under irradiation. These results indicate the co-loaded

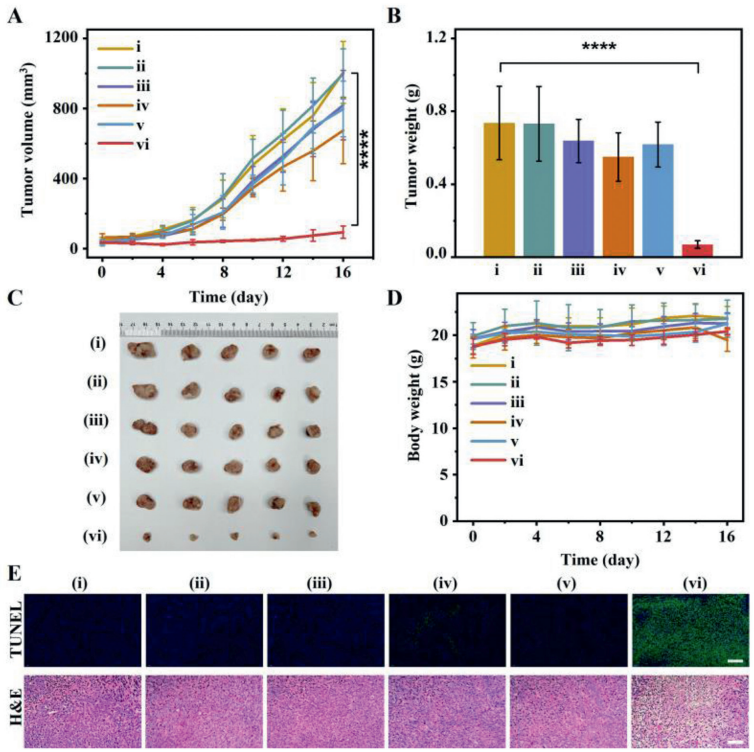

Fig. 4. (A) Tumor volumes of the mice upon different treatments: (i) PBS + light, (ii) Pt@BSA, (iii) Ru@BSA, (iv) Ru@BSA + light, (v) Ru/Pt@BSA, (vi) Ru/Pt@BSA + light. (B) Average tumor weights of the mice after different treatments for 16 days. (C) Tumor sizes of the mice after different treatments for 16 days. (D) Body weight changes of the mice during treatments. (E) H&E and TUNEL staining images of tumor slices obtained from different groups. Scale bars: 200 μm. Data were presented as mean ± SD ($n = 5$). $^{****}P < 0.0001$ (two-tailed Student's *t*-test).

Pt NPs can significantly strengthen the anticancer activity of Ru1 under hypoxic conditions, which is consistent with the MTT results.

Based on the efficient and targeted anticancer activity of Ru/Pt@BSA *in vitro*, we then investigated the performance *in vivo* utilizing a 4T1 tumor-bearing mouse model as a proof of concept. All animal experiments were carried out with the permission of the Ethics Committee of Technical Institute of Physics and Chemistry, CAS (IACUC Issue No.: IACUC-IPC-22058). When the tumors grew up to about 50 mm^3, all the mice were randomly allocated into 6 groups with 5 mice in each group: (i) PBS + light, (ii) Pt@BSA, (iii) Ru@BSA, (iv) Ru@BSA + light, (v) Ru/Pt@BSA, (vi) Ru/Pt@BSA + light. The agents were injected *via* the tail vein with dosages of 25 mg/kg (about 1.0 mg/kg in Ru1 or 2.1 mg/kg in Pt when involved). Six hours after each injection, the tumors of the light groups were irradiated with a 520 nm laser (100 mW/cm^2) for 10 min. As shown in Fig. 4A, the tumor volumes of PBS + light group increased by 20 times over the therapeutic course. Pt@BSA, Ru@BSA, Ru@BSA + light and Ru/Pt@BSA displayed very poor anticancer activity, and only Ru/Pt@BSA + light could significantly inhibit tumors growth. Similar results were also observed for the tumor weights and sizes (Figs. 4B and C). These results confirm that the presence of Pt NPs can greatly enhance the photoactivated anticancer activity of Ru1 *in vivo*. The body weights of the mice before and after treatment did not change obviously (Fig. 4D). All the mice were sacrificed after 16 days, and the tumor tissues and the main organs (including heart, live, spleen, lung and kidney) were collected and stained by hematoxylin and eosin (H&E). Besides, terminal deoxynucleotidyl transferase dUTP nick end labeling (TUNEL) staining was also applied for the tumor tissues. As expected, only the tumor tissues after treatment by Ru/Pt@BSA + light were severely damaged (Fig. 4E). The main organs in all groups did not show obvious tissue damage/abnormality (Fig. S22 in Supporting information), which indicates the excellent biocompatibility of these agents.

In conclusion, photo-catalytic NAD(P)H oxidation as a novel anticancer mechanism has attracted much attention in the very recent years. However, the general oxygen-dependent mechanism may heavily limit the efficacy in hypoxic tumor tissues. In this work, to strengthen the photo-catalytic NAD(P)H oxidation activity of Ru1 in hypoxia, Pt NPs with CAT-like and HEC activities were introduced as a powerful assistant. The CAT-like activity of Pt NPs can transform the original and *in situ* formed H_2O_2 once again into O_2, thus relieving tumor hypoxia and also realizing cyclic utilization (at least in part) of precious oxygen in hypoxia. Moreover, the HEC activity of Pt NPs can provide an oxygen-independent pathway for photo-catalytic oxidation of NAD(P)H. *Via* co-encapsulation of Ru1 and Pt NPs in BSA with tumor targeting ability, the resultant Ru/Pt@BSA can photo-catalyze NADH oxidation in hypoxic (3% O_2) and even oxygen-free solutions. The results *in vitro* displayed that Ru/Pt@BSA upon irradiation can effectively deplete intracellular NAD(P)H, produce ROS and selectively kill cancer cells under hypoxic conditions, while the performances of Ru@BSA were quite poor under the same conditions. Finally, Ru/Pt@BSA could also greatly inhibit tumor growth *in vivo*. Our results may provide new sights for efficient photo-catalytic oxidation of NAD(P)H and targeted cancer treatment under hypoxic conditions.

Declaration of competing interest

The authors declare that they have no known competing financial interests or personal relationships that could have appeared to influence the work reported in this paper.

Acknowledgments

This work was financially supported by Research Equipment Development Project of Chinese Academy of Sciences (No. YJKYYQ20210014). We really appreciate Dr. Wuyi Xiao, from CAS Key Laboratory of Bio-inspired Materials and Interfacial Science, for offering help with the animal experiment.

Supplementary materials

Supplementary material associated with this article can be found, in the online version, at doi:10.1016/j.cclet.2023.108317.

References

[1] Q. Sun, Z. Wang, B. Liu, et al., Coord. Chem. Rev. 451 (2022) 214267.
[2] H. Sung, J. Ferlay, R.L. Siegel, et al., CA Cancer J. Clin. 71 (2021) 209–249.
[3] F. Bray, J. Ferlay, I. Soerjomataram, et al., CA Cancer J. Clin. 68 (2018) 394–424.
[4] S.L. Li, P. Jiang, F.L. Jiang, Y. Liu, Adv. Funct. Mater. 31 (2021) 2100243.
[5] R.W. Johnstone, A.A. Ruefli, S.W. Lowe, Cell 108 (2022) 153–164.
[6] Y. Zhou, S. Fan, L. Feng, X. Huang, X. Chen, Adv. Mater. 33 (2021) 2104223.
[7] W. Bao, M. Liu, J. Meng, et al., Nat. Commun. 12 (2021) 6399.
[8] K. Ni, T. Aung, S. Li, et al., Chem 5 (2019) 1892–1913.
[9] K. Ni, T. Luo, G.T. Nash, W. Lin, Acc. Chem. Res. 53 (2020) 1739–1748.
[10] W. Wu, L. Yu, Q. Jiang, et al., J. Am. Chem. Soc. 141 (2019) 11531–11539.
[11] S. Li, B. Xu, M. Lu, et al., Adv. Mater. 34 (2022) e2202609.
[12] Y. Zhao, X. Liu, X. Liu, et al., Front. Immunol. 13 (2022) 955920.
[13] C. Wang, Y. Zhang, H. Li, et al., Chin. Chem. Lett. 33 (2022) 2447–2450.
[14] H. Wang, Zhang H, W. Xing, et al., Chin. Chem. Lett. 33 (2022) 4033–4036.
[15] D. Xu, Q. Zhou, X. Dal, et al., Chin. Chem. Lett. 33 (2022) 851–854.
[16] H. Huang, S. Banerjee, K. Qiu, et al., Nat. Chem. 11 (2019) 1041–1048.
[17] A. Chiarugi, C. Dölle, R. Felici, M. Ziegler, Nat. Rev. Cancer 12 (2012) 741–752.
[18] A.O. Elzoghby, W.M. Samy, N.A. Elgindy, J. Control. Release 157 (2012) 168–182.
[19] Z. Fan, Y. Rong, T. Sadhukhan, et al., Angew. Chem. Int. Ed. 61 (2022) e202202098.
[20] C. Huang, C. Liang, T. Sadhukhan, et al., Angew. Chem. Int. Ed. 60 (2021) 9474–9479.
[21] L. Lee, K. Lo, J. Am. Chem. Soc. 144 (2022) 14420–14440.
[22] A.K. Mengele, D. Weixler, A. Chettri, et al., Chem. Eur. J. 27 (2021) 16840–16845.
[23] S. Qi, Z. Jin, Y. Jian, et al., Chem. Commun. 57 (2021) 4162–4165.
[24] C. Liang, J. Xie, S. Luo, et al., Nat. Commun. 12 (2021) 5001.
[25] X. Da, Z. Wang, Y. Jian, et al., Inorg. Chem. Front. 9 (2022) 2544–2556.
[26] K. Teng, L. Niu, N. Xie, Q. Yang, Nat. Commun. 13 (2022) 6179.
[27] M. Li, K.H. Gebremedhin, D. Ma, et al., J. Am. Chem. Soc. 144 (2022) 163–173.
[28] M. Li, Y. Xu, Z. Pu, et al., Proc. Natl. Acad. Sci. U. S. A. 119 (2022) e2210504119.
[29] H. Fan, G. Yan, Z. Zhao, et al., Angew. Chem. Int. Ed. 55 (2016) 5477–5482.
[30] S. Hou, Y.E. Gao, X. Ma, et al., Chem. Eng. J. 416 (2021) 129037.
[31] F. Jiang, B. Ding, S. Liang, et al., Biomaterials 268 (2021) 120545.
[32] P. Zhao, Z. Tang, X. Chen, et al., Mater. Horizons. 6 (2019) 369–374.
[33] K. Teng, Chen W, L. Niu, et al., Angew. Chem. Int. Ed. 60 (2021) 19912–19920.
[34] K. Teng, L. Niu, Q. Yang, et al., Chem. Sci. 13 (2022) 5951–5956.
[35] Y. Cheng, H. Cheng, C. Jiang, et al., Nat. Commun. 6 (2015) 8785.
[36] R. Liang, L. Liu, H. He, et al., Biomaterials 177 (2018) 149–160.
[37] F. Shen, C. Zhang, Z. Cai, et al., Chem. Eng. J. 438 (2022) 135556.
[38] Z. Wang, Y. Yan, C. Li, et al., ACS Nano 16 (2022) 9019–9130.
[39] L. Gong, Y. Zhang, J. Zhao, et al., Small 18 (2022) e2107656.
[40] F. Bonnay, A. Veloso, V. Steinmann, et al., Cell 182 (2020) 1490–1507.
[41] L. Liu, Y. Wang, Y. Zhao, et al., Adv. Funct. Mater. 32 (2022) 2112207.
[42] T. Zhang, C. Pei, G. Sun, et al., Angew. Chem. Int. Ed. 61 (2022) e202201453.
[43] S. Wang, Y. Pang, S. Hu, et al., Chem. Eng. J. 451 (2023) 138864.
[44] C. Zhang, X. Guo, X. Da, et al., Dalton Trans. 50 (2021) 7715–7724.
[45] X. Liu, X. Dong, S. Yang, et al., Adv. Sci. 8 (2021) 2003679.
[46] Y. Teow, S. Valiyaveettil, Nanoscale 2 (2010) 2607–2613.
[47] P.R. Van, M.J. Mckelvy, W.S. Glaunsinger, J. Solid State Chem. 67 (1986) 151–169.